The Journal of Experimental Biology 215, 22-28

doi:10.1242/jeb.060095

RESEARCH ARTICLE

Oxygen utilization and the branchial pressure gradient during ram ventilation of the shortfin mako, *Isurus oxyrinchus*: is lamnid shark–tuna convergence constrained by elasmobranch gill morphology?

Nicholas C. Wegner[1,*], N. Chin Lai[1,2], Kristina B. Bull[1] and Jeffrey B. Graham[1]

[1]Center for Marine Biotechnology and Biomedicine, Marine Biology Research Division, Scripps Institution of Oceanography, University of California San Diego, La Jolla, CA 92093, USA and [2]Department of Medicine, University of California San Diego, La Jolla, CA 92093, USA

*Author for correspondence (nwegner@ucsd.edu)

Accepted 23 September 2011

SUMMARY

Ram ventilation and gill function in a lamnid shark, the shortfin mako, *Isurus oxyrinchus*, were studied to assess how gill structure may affect the lamnid–tuna convergence for high-performance swimming. Despite differences in mako and tuna gill morphology, mouth gape and basal swimming speeds, measurements of mako O_2 utilization at the gills (53.4±4.2%) and the pressure gradient driving branchial flow (96.8±26.1 Pa at a mean swimming speed of 38.8±5.8 cm s^{-1}) are similar to values reported for tunas. Also comparable to tunas are estimates of the velocity (0.22±0.03 cm s^{-1}) and residence time (0.79±0.14 s) of water though the interlamellar channels of the mako gill. However, mako and tuna gills differ in the sites of primary branchial resistance. In the mako, approximately 80% of the total branchial resistance resides in the septal channels, structures inherent to the elasmobranch gill that are not present in tunas. The added resistance at this location is compensated by a correspondingly lower resistance at the gill lamellae accomplished through wider interlamellar channels. Although greater interlamellar spacing minimizes branchial resistance, it also limits lamellar number and results in a lower total gill surface area for the mako relative to tunas. The morphology of the elasmobranch gill thus appears to constrain gill area and, consequently, limit mako aerobic performance to less than that of tunas.

Key words: mako shark, tuna, elasmobranch gill, branchial resistance, interbranchial septum, evolutionary convergence, aerobic performance.

INTRODUCTION

The shortfin mako, *Isurus oxyrinchus* (Rafinesque 1810), and other sharks in the family Lamnidae are convergent with tunas (Family Scombridae) in a number of features related to fast, continuous swimming. Both groups have a streamlined, fusiform body, a unique positioning of the aerobic (red) musculature, and the ability to maintain core body temperatures above ambient seawater, thereby increasing muscle power output and accelerating metabolically mediated processes (Carey et al., 1971; Altringham and Block, 1997; Bernal et al., 2001a; Graham and Dickson, 2001). Lamnids and tunas are also obligate ram ventilators, meaning they depend on continuous swimming to force water through the gills. Relative to most other fishes, both lamnid sharks and tunas have high metabolic demands (Brill, 1979; Brill, 1987; Brill and Bushnell, 1991; Dewar and Graham, 1994; Korsmeyer and Dewar, 2001; Sepulveda et al., 2007). However, it is now well established that lamnid aerobic capacity is less than that of tunas. Lamnids have lower mitochondrial densities and aerobic enzyme activities (Bernal et al., 2003b), smaller gill surface areas (Muir, 1969; Emery and Szczepanski, 1986; Wegner et al., 2010a; Wegner et al., 2010b) and lower amounts of red muscle (Graham et al., 1983; Bernal et al., 2003a). Water-tunnel studies also indicate that the maximum sustainable swimming speed of the shortfin mako is much lower than that of tunas (Dewar and Graham, 1994; Blank et al., 2007; Sepulveda et al., 2007).

Recent analysis of mako gill morphology suggests that structural features inherent to the elasmobranch gill potentially limit respiratory surface area and may thereby restrict oxygen uptake and the aerobic scope of lamnid sharks in comparison to tunas (Wegner et al., 2010b). The elasmobranch gill differs from that of bony fishes in having interbranchial septa that bind together the anterior and posterior hemibranchs of each gill arch and extend out to the lateral edge of the body to form the gill flaps (Fig. 1A,B). Each interbranchial septum thus provides an extended base of attachment for the gill filaments, and it is this characteristic that gave rise to the term elasmobranch (=strapped gill). Tunas and other teleosts have greatly reduced branchial septa; the filaments of each hemibranch are anchored to the gill arch but extend into the branchial cavity without septal support for the majority of their length (Fig. 1C,D). This difference in gill structure markedly affects the path of water flow. In tunas, water that passes through the interlamellar channels freely exits the branchial chamber through the opercular opening. In contrast, water exiting the interlamellar channels of a lamnid impinges on the branchial septum where it is turned and forced through septal channels that open just inside the gill slits. Wegner et al. (Wegner et al., 2010b) suggested that the added resistance to water flow incurred at these channels may prevent lamnids from having the high lamellar frequency (i.e. the high number of lamellae per length of filament) required to achieve tuna-like gill surface areas (i.e. more, closely spaced lamellae would further increase gill resistance). Tunas, which have a greatly reduced branchial septum and therefore lack the added resistance of the septal channels, have a lamellar frequency that is twice that of lamnids

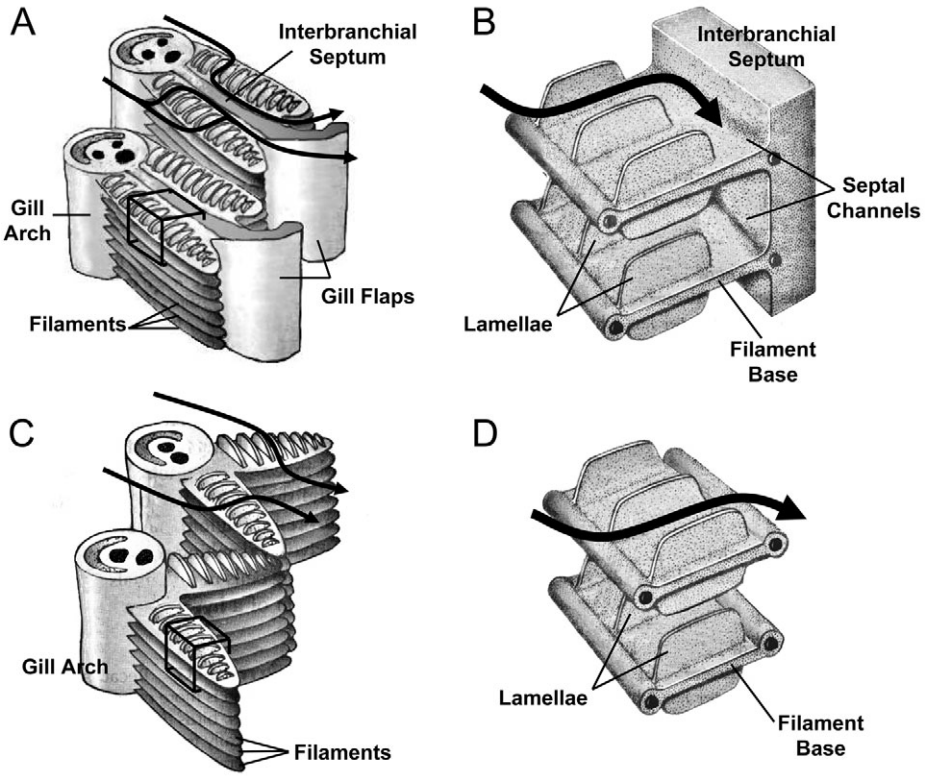

Fig. 1. Simplified drawings of the basic structural features of the elasmobranch (A,B) and teleost (C,D) gill. B and D are enlarged views of the boxes in A and C, respectively. The path of water flow through the gills is indicated by arrows.

and this is the primary feature of the gills leading to their larger respiratory surface area.

Although morphometric studies suggest that lamnid gill area (and, ultimately, the maximum consumption rate of oxygen) may be limited by flow constraints associated with the elasmobranch gill, there have been no measurements or hydrodynamic estimates of septal channel resistance, and thus its effect on gill dimensions and respiratory function has not been quantified. In contrast, ventilatory flow and gill function in tunas has been well studied. Brown and Muir (Brown and Muir, 1970) first examined tuna ram ventilation by tracing the path of water through the oral and branchial cavities (from the mouth to opercula) and used corresponding morphological measurements to estimate the pressure gradient required to drive ventilatory flow. These initial pressure-drop estimates were verified with *in vivo* measurements on anesthetized skipjack tuna, *Katsuwonus pelamis*, by Stevens (Stevens, 1972), who also documented relatively high O_2 utilizations (i.e. the percent of ventilatory O_2 absorbed at the gills) in swimming tunas despite their large ventilatory volumes. Further morphological work has quantified micro-flow characteristics of the tuna ventilatory stream, including estimates of the velocity, Reynold's number (*Re*) and residence time of water along the gas-exchange surfaces (Stevens and Lightfoot, 1986). Building upon the methods of these previous studies, the present study reports *in vivo* measurements of O_2 utilization and the branchial pressure gradient determined for small shortfin makos swimming in a water tunnel and combines these findings with morphometric data to model aspects of lamnid gill function in comparison to tunas.

MATERIALS AND METHODS

Mako shark collection, transport and experimentation were conducted in accordance with protocol S00080 of the University of California, San Diego Institutional Animal Care and Use Committee.

Specimen collection

Six small shortfin makos (4.62–7.32 kg, 76.0–89.0 cm fork length) were collected over an eight week period 8–13 km offshore of Scripps Institution of Oceanography (SIO), La Jolla, CA. Five were captured by chumming, in which a shark attracted to the boat was fed a piece of bait on a barbless hook and pulled close enough (usually without setting the hook) to be dip-netted. One mako (mako 2) was caught by trolling with heavy fishing gear (fight time was less than 1 min).

Each shark was transported (30–50 min in duration) to the laboratory in a rectangular (110×34×51 cm, length×width×height) tank used in previous studies (Donley et al., 2005; Sepulveda et al., 2007) that was filled halfway with 901 of seawater. This tank has a recirculating and aerated flow system that pumps water through a funnel placed over the snout of the shark to induce ventilation. Restraints on the anterior half of the body secured the head of the shark in the funnel while allowing it to make regular tail movements. At SIO, each shark was placed in a 5.4 m diameter, 24,5001 holding tank where it swam freely for 1–24 h.

Water-tunnel experiments

Each shark was transferred from the holding tank into the working section (200×51×42 cm) of a 30001 Brett-type water tunnel used in previous studies (Graham et al., 1990; Dewar and Graham, 1994; Bernal et al., 2001b; Dowis et al., 2003; Sepulveda et al., 2003; Donley et al., 2005; Sepulveda et al., 2007). Water flow through the tunnel was driven by a 45.7 cm (18 in) propeller connected to a 40 hp variable-speed electric motor. An upstream diffuser–contraction section and honeycomb collimator streamlined water entering the working section, and multiple airstones were used to maintain O_2 saturation. Water velocity in the working section was monitored by a FlowTracker Handheld Acoustic Doppler Velocimeter (SonTek, San Diego, CA, USA). Continuous adjustment of water speed over a period of 1–2 h was required to

condition the shark to swim steadily against the current with minimal change in positioning within the working section.

Once the shark was swimming regularly, measurements of O_2 utilization were determined using a custom-made polarographic oxygen electrode (Warner Instruments, Hamden, CT, USA; probe length 70 mm, tip diameter 2 mm, equilibration time ~15 s) connected to an oxygen meter (Strathkelvin Instruments Model 781, North Lanarkshire, UK) by a 3 m cable. The oxygen partial pressure (P_{O2}) of post-branchial water was sampled at three locations (top, middle, and bottom) in each gill slit by guiding the swimming shark to the top of the working section and advancing the O_2 probe approximately 5–10 mm into the slit. This distance was far enough to eliminate errors associated with the non-respiratory water flow along the body surface, but not too far inside the slit as to contact the gill filaments. Following the three regional measurements on a slit, the O_2 sensor was withdrawn and the background O_2 of the swim tunnel water was resampled while the shark was allowed to continue swimming. Once regional measurements on all five gill slits had been made, a flexible plastic cowling contoured to cover all slits on one side of the body was attached to the swimming shark using two elastic bands. The shark was allowed to swim with the cowling for 1–2 min, following which the O_2 sensor was advanced into the posterior-facing opening to obtain an integrated measurement of O_2 utilization for all five slits. After recalibration of the O_2 sensor, both the regional and integrated (cowling) O_2 measurements were replicated. The required time to make one series of these measurements (i.e. 15 gill slit + one cowling measurement) was approximately 30 min.

Following the O_2 utilization measurements, the pressure gradient between the mouth and the gill slits was determined using two in-series Millar pressure transducers (SPR-1000 1 French, SPR-671 2 French) connected to an MPVS-300 amplifier (Millar Instruments, Houston, TX, USA) interfaced with a DATAQ acquisition system (DATAQ Instruments, Akron, OH, USA). Pressure transducers were threaded into position through guide catheters (5 mm diameter), one attached to the tip of the tongue and entering the branchial cavity through the first gill slit, and a second attached approximately 5 mm inside the third gill slit along the same horizontal plane. The head (strain-gauge) of each transducer was positioned to emerge approximately 2 mm outside the end of each catheter. To maintain consistent pressure transducer positioning within the catheters and minimize pressure artifacts associated with the height of the water column (i.e. manometric height), each shark was placed in a harness that minimized changes in its vertical position (depth) and pitch (relative vertical positioning of the in-series pressure transducers) but did not interfere with swimming motions. Once the shark was situated in the harness and the pressure transducers were in place, water-tunnel flow was momentarily stopped to 'zero' each pressure transducer. The shark was then exposed to a series of water-flow velocities (up to 73 cm s^{-1}) and the resulting pressures at the mouth and third gill slit were recorded.

Flow-field dimensions

Following branchial pressure measurements, each shark was euthanized by severing the spinal cord immediately posterior to the chondrocranium. The head of each specimen was fixed in 10% formalin buffered in seawater and used for morphological measurements needed to quantify water flow through the branchial chamber. These included: (1) mouth cross-sectional area to determine ventilation volume, (2) cross-sectional area between the gill arches (=gill bars) to calculate water velocity at this location, and (3) gill dimensions (total filament length, lamellar frequency, and lamellar length, height and thickness) to estimate water velocity and the theoretical pressure gradient of ventilatory flow through the interlamellar channels.

For each mako, mouth cross-sectional area was determined by comparing post-mortem head measurements with digital images of gape while swimming in the tunnel. A silicon cast made for one side of the branchial chamber enabled measurement of the cross-sectional area between each gill arch. Gill dimensions were determined using methods described by Wegner et al. (Wegner et al., 2010b). Total filament length was calculated by counting all of the gill filaments from one side of the branchial apparatus. Filaments on each gill hemibranch were divided into bins of 20 and the medial filament from each bin (i.e. the 10th, 30th, 50th, etc.) was measured and assumed to represent the mean filament length for that bin. The total length of the filaments in each bin was calculated, and all of the bins were added to determine the total filament length for one side of the branchial chamber; this quantity was then doubled to account for filaments on the opposite side.

To determine lamellar frequency and mean lamellar length, the medial filament of each bin on the third gill arch was removed, and digital images of lamellae at the base, middle, and tip were acquired using a camera mounted on a light microscope. Lamellae from these sections were then dissected from each filament and photographed to determine mean lamellar height. Finally, scanning electron microscopy (SEM) was used to determine lamellar thickness. Randomly selected sections of the filaments from the third gill arch were rinsed in deionized water, slowly dehydrated in tert-butyl alcohol (25% increments over 24 h and rinsed twice at 100%) and frozen in the alcohol at 4°C. Frozen sections were then placed in a freeze dryer until all of the alcohol was removed. Longitudinal cross-sections through the freeze-dried filaments were sputter coated with gold-palladium, mounted perpendicular to the SEM field-of-view, and photographed using an FEI Quanta 600 SEM (Hillsboro, OR, USA) under high-vacuum mode. Lamellar thickness was determined for 20 lamellae from each specimen. Digital images of each lamellar parameter were analyzed using ImageJ software (National Institutes of Health, Bethesda, MD, USA).

Statistics

Regional measurements of O_2 utilization were compared using a *t*-test with a significance criterion of $P<0.05$. The relationship between the branchial pressure gradient and swimming speed was determined by least-squares analysis. Branchial dimensions and water-flow parameters combined for all six sharks are given as means ± s.d.

RESULTS

O_2 utilization

Regional measurements of O_2 utilization combined for all six makos are shown in Fig. 2. The percentage of gill-O_2 utilization measured at the mid-region of each slit was significantly less than that at the dorsal and ventral slit positions (e.g. at the first gill slit, 20.1% utilization at the middle position is significantly less than 46.0% and 49.7% at the dorsal and ventral locations, respectively). O_2 utilizations measured at the dorsal and ventral positions did not differ significantly, with the exception of slit 5 where ventral utilization (75.5%) was significantly higher than that at the dorsal position (62.4%). The tabular data in Fig. 1 show the mean O_2 utilization for each slit calculated by combining the three regional measurements (top, middle and bottom) for all six makos. The mean O_2 utilization measured at the first gill slit (38.6±17.1) was significantly less than that determined at slits 2–5. Utilization measured at gill slit 2

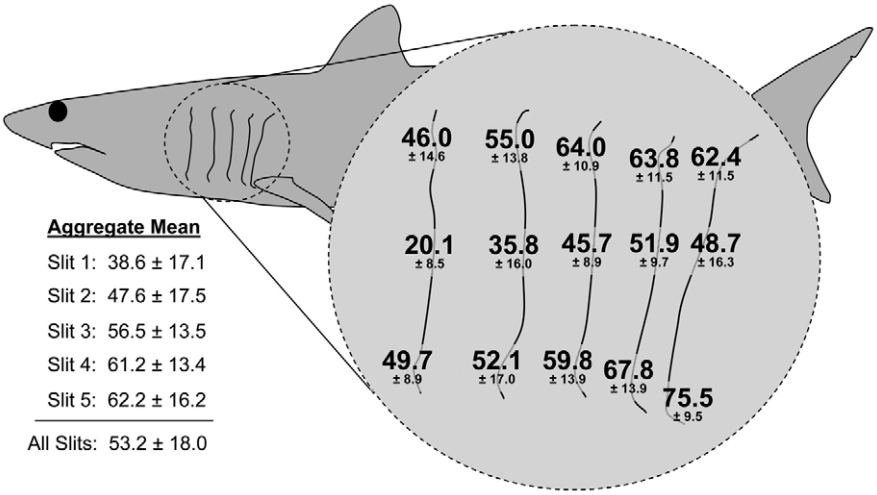

Fig. 2. Regional measures of gill-O_2 utilization for six makos swimming at 38.8±5.8 cm s^{-1} (0.43±0.06 TL s^{-1}). Tabular data (left) show the aggregate mean O_2 utilization for each gill slit. Data are means ± s.d.

(47.6±17.5) was significantly greater than that of slit 1, but significantly less than that of slits 3–5. O_2 utilizations determined at gill slits 3–5 did not differ significantly. The aggregate mean utilization of all slit measurements for all six sharks (53.2±18.0%) was consistent with the integrated mean utilization determined for all slits using the cowling (53.4±4.2%). Total and regional measurements of O_2 utilization did not differ significantly between sharks.

Pressure measurements

The total pressure differential (ΔP_{tot}, Pa) measured between the front of the buccal cavity and the third gill slit is shown in relation to swimming speed (v_s) in Fig. 3 and results in the regression equation:

$$\Delta P_{tot} = 0.1347 v_s^{1.7938}. \quad (1)$$

Much of the variation in these data is likely attributed to slight changes in the pitch of the shark. The harness used to stabilize mako position during these measurements limited alterations in body angle to ±2 deg relative to horizontal; this correlates to a 0.4–0.6 cm change in the relative height of the pressure transducers and a potential pressure change of 39–59 Pa. However, some values of ΔP_{tot} exceeded this expected range of variation. Pressure differentials that were less than zero (i.e. pressure at the third gill slit was higher than that at the mouth) or greater than twice the dynamic pressure predicted at a given swimming speed ($=0.5\rho v^2$, where ρ is the density of seawater and v is water velocity) were considered transducer errors and were not included in the analysis. These errors may have been caused by changes in the relative positioning of pressure transducers associated with their extension from the guide catheters during swimming. [Note: a power-law regression equation was chosen to represent the pressure–velocity relationship shown in Fig. 3 as its R^2 value (0.6237) suggests a better fit than that of a linear function forced through the origin (R^2=0.5373).]

Branchial water flow

The preferred mako swimming speed in the water tunnel ranged from 32.7 to 45.5 cm s^{-1} [mean 38.8±5.8 cm s^{-1}, 0.43±0.06 total lengths (TL) s^{-1}], which is similar to the cruising speed observed for makos by Sepulveda et al. [0.44 TL s^{-1} (Sepulveda et al., 2007)]. Table 1 integrates these basal swim speeds with measurements of branchial chamber and gill morphology, the pressure gradient, and O_2 utilization in order to quantify aspects of the mako ram-ventilatory stream. Thus, shown in Table 1 are estimates of branchial water-flow parameters at different locations along the respiratory tract, including details of water velocity, *Re* and residence time in the interlamellar channels. Also estimated are the contributions of different sections of the respiratory-flow pathway to branchial resistance.

DISCUSSION

Mako branchial water flow

The mako ram-ventilatory stream begins with the entrance of water into the mouth, where the maximum ventilation volume ($\dot{V}_{gmax}$, $cm^3 s^{-1}$) is determined by:

$$\dot{V}_{gmax} = A_m v_s, \quad (2)$$

where A_m is the cross-sectional area of the mouth (cm^2) and v_s is equal to 38.8±5.8 cm s^{-1} (Table 1). However, because of branchial resistance, the velocity of the ram-ventilatory flow entering the mouth is less than swimming speed (i.e. branchial resistance creates

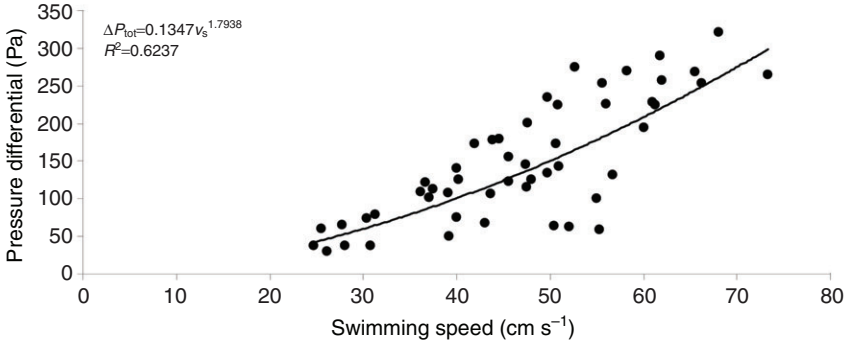

Fig. 3. Pressure differential (ΔP_{tot}) between the front of the buccal cavity and the third gill slit for six makos (4.6–7.3 kg) swimming at different speeds (v_s).

Table 1. Parameters of ram ventilation for six shortfin makos swimming in a water tunnel

Variable	Symbol	Data source	Mako 1	Mako 2	Mako 3	Mako 4	Mako 5	Mako 6	Mean ± s.d.
Shark measurements									
Mass (kg)	M	Direct measurement	4.62	4.71	5.01	6.77	6.95	7.32	–
Fork length (cm)	FL	Direct measurement	77.0	77.5	76.0	88.5	89.0	89.0	–
Total length (cm)	TL	Direct measurement	84.0	85.0	85.0	96.5	95.0	97.0	–
Experimental parameters									
Water temperature (°C)	T	Direct measurement	17.9	19.4	19.3	17.0	18.2	17.7	–
Water O_2 concentration (mg O_2 l^{-1})	C_{wO_2}	Direct measurement	7.8	7.6	7.6	8.0	7.8	7.8	–
Swimming and O_2 consumption									
Mean swimming velocity (cm s^{-1})	v_s	Direct measurement	40.2	34.7	32.7	45.5	45.7	34.1	38.8±5.8
Mean swimming velocity (TL s^{-1})	$v_{s\text{-}TL}$	v_s / TL	0.48	0.41	0.38	0.47	0.48	0.35	0.43±0.06
O_2 consumption (mg O_2 kg^{-1} h^{-1})	$\dot{V}_{O_2}$	$10^{(2.0937+0.97 v_{s\text{-}TL})}$	361.3	308.8	293.0	355.7	363.3	272.1	325.7±39.5
O_2 utilization (%)	U	Direct measurement	58.1	46.3	52.3	52.0	56.2	55.6	53.4±4.2
Oral cavity water flow									
Mouth cross-sectional area (cm^2)	A_m	Direct measurement	4.6	4.5	4.6	4.8	5.2	5.9	4.9±0.5
Max ventilation volume (cm^3 s^{-1})	$\dot{V}_{gmax}$	$v_s A_m$	184.9	157.4	150.4	218.6	237.6	201.2	191.7±34.2
Ventilation volume (cm^3 s^{-1})	$\dot{V}_g$	$(M\dot{V}_{O_2}) / (C_{wO_2} U)$	102.3	114.8	102.6	160.8	160.0	127.9	128.1±26.8
Water velocity entering mouth (cm s^{-1})	v_m	$\dot{V}_g / A_m$	22.2	25.3	22.3	33.5	30.8	21.7	26.0±5.0
Area between gill arches (cm^2)	A_{ga}	Direct measurement	6.6	7.6	8.2	7.5	7.7	10.7	8.1±1.4
Water velocity at gill arches (cm s^{-1})	v_{ga}	$\dot{V}_g / A_{ga}$	15.5	15.1	12.4	21.4	20.7	11.9	16.2±4.1
Gill dimensions									
Total filament length (cm)	L_{fil}	Direct measurement	6986.4	7287.8	7580.8	8026.4	8186.8	8288.8	7726.2±525.2
Lamellar frequency (mm^{-1})	f_{lam}	Direct measurement	16.17	15.77	14.95	14.00	14.47	15.68	15.17±0.84
Total number of lamellar channels	n_{lc}	$2 f_{lam} L_{fil}$	2,259,011	2,297,843	2,267,023	2,246,638	2,368,867	2,599,053	2,339,739± 134,402
Lamellar channel length (mm)	l	Direct measurement	1.57	1.50	1.75	1.73	1.97	1.74	1.71±0.16
Lamellar channel height (mm)	b	Direct measurement	0.435	0.372	0.452	0.456	0.508	0.443	0.444±0.044
Lamellar thickness (μm)	t	Direct measurement	11.26	9.31	10.43	10.36	10.87	9.40	10.27±0.78
Lamellar channel width (μm)	d	$[1000 - (t f_{lam})] / f_{lam}$	50.60	54.12	56.45	61.10	58.25	54.38	55.82±3.64
Total lamellar channel cross-sectional area (cm^2)	A_{lc}	$n_{lc} b d$	497.2	462.4	578.5	625.9	701.0	626.3	581.9±89.0
Gill water flow									
Interlamellar water velocity (cm s^{-1})	v_{lc}	$\dot{V}_g / A_{lc}$	0.21	0.25	0.18	0.26	0.23	0.20	0.22±0.03
Interlamellar Reynold's number	Re	$(0.5 \rho d v_{lc}) / \mu$	0.05	0.07	0.05	0.08	0.07	0.06	0.06±0.01
Interlamellar water residence time (s)	R	l / v_{lc}	0.76	0.60	0.99	0.67	0.86	0.85	0.79±0.14
Water pressure									
Total head (Pa)	H_{tot}	$0.5 \rho v_s^2$	82.8	61.7	54.8	106.1	107.0	59.6	78.7±23.6
Dynamic pressure at mouth (Pa)	H_d	$0.5 \rho v_m^2$	25.4	32.8	25.5	57.4	48.5	24.1	35.6±14.1
Total pressure drop (Pa)	ΔP_{tot}	$0.1347 v_s^{1.7938}$	101.7	78.1	70.2	126.9	127.9	75.7	96.8±26.1
Buccal cavity pressure drop (Pa)	ΔP_{bc}	$0.15 H_d$	3.8	4.9	3.8	8.6	7.3	3.6	5.3±2.1
Interlamellar pressure drop (Pa)	ΔP_{lc}	$(12 \mu v_{lc} l) / d^2$	15.2	15.2	11.7	14.3	15.9	14.5	14.4±1.5
Septal channel pressure drop (Pa)	ΔP_{sc}	$\Delta P_{tot} - (\Delta P_{bc} + \Delta P_{lc})$	82.7	57.9	54.7	104.0	104.8	57.6	77.0±23.6
Negative pressure at gills slits (Pa)	P_{gs}	$H_{tot} - \Delta P_{tot}$	–18.8	–16.4	–15.4	–20.8	–20.9	–16.1	–18.1±2.5
Pressure coefficient at gills slits	C_p	P_{gs} / H_{tot}	–0.23	–0.27	–0.28	–0.20	–0.20	–0.27	–0.24±0.04
Constants									
Dynamic viscosity of water (cm^2 s^{-1})	μ	0.01							
Density of seawater (kg l^{-1})	ρ	1.025							

Equation references: $\dot{V}_{O_2}$ (Sepulveda et al., 2007), Re (Stevens and Lightfoot, 1986), $\dot{V}_g$ and ΔP_{lc} (Brown and Muir, 1970).

a slight water-displacing bow wave) (Brown and Muir, 1970); thus, true ventilation volume ($\dot{V}_g$) is calculated by:

$$\dot{V}_g = (M\dot{V}_{O_2}) / (C_{wO_2} U), \quad (3)$$

where M is fish mass (kg), $\dot{V}_{O_2}$ is oxygen consumption (mg O_2 kg^{-1} h^{-1}), C_{wO_2} is the concentration of oxygen in the water (mg O_2 l^{-1}) and U is percent O_2 utilization (Brown and Muir, 1970). Values for these variables are reported in Table 1 for each shark, and estimates for $\dot{V}_g$ using this equation average 33% less than $\dot{V}_{gmax}$. Water velocity entering the mouth (v_m=26.0±5.0 cm s^{-1}) is thus approximately two-thirds the swimming speed.

The velocity of the ventilatory stream at subsequent locations along the oral and branchial cavities is determined by the law of continuity:

$$\dot{V}_g = A_1 v_1 = A_2 v_2, \quad (4)$$

where the ventilation volume is the product of any cross-sectional area (A) through which the flow is passing and the velocity (v) at that point. At the gill arches, water velocity is further reduced to approximately 40% of swimming speed (16.2±4.1 cm s^{-1}; Table 1). Assuming the entire ventilatory stream subsequently enters the interlamellar channels, water velocity along the respiratory exchange surfaces is reduced by two orders of magnitude to approximately 0.6% of swimming speed (0.22±0.03 cm s^{-1} at a mean swimming speed of 38.8±5.8 cm s^{-1}; Table 1).

The regional differences in gill-O_2 utilization shown in Fig. 2 could indicate that flow is not evenly distributed to the lamellae and thus interlamellar velocity may vary regionally. Specifically, the lower utilizations observed at the first and second gill arches and near the mid-slit position on each arch could reflect increased water flow at these locations. If branchial flow were sufficiently strong, the tips of the gill filaments from opposing hemibranchs

could be forced apart to allow some flow to bypass the respiratory surfaces, creating anatomical deadspace. However, good agreement between the aggregate mean O_2 utilization for all regional measurements (53.2±18.0%; Fig. 1) and the integrated utilization estimate made with the cowling (53.4±4.2%; Table 1) indicates that the lower O_2 utilizations at gill arches 1 and 2 and near the middle of each slit do not disproportionately contribute to the aggregate mean utilization (as would be expected if a larger volume of water were passing through or shunting around the gills at these locations). Therefore, these regional differences in O_2 utilization may reflect variation in blood perfusion through the gills.

Pressure differential of the ventilatory stream

The total pressure differential of the ventilatory stream for each mako swimming at its mean speed is determined by Eqn 1 and reported in Table 1. The components of this pressure differential can be further examined using Bernoulli's equation for fluid dynamics:

$$P + 0.5\rho v^2 + \rho g z = \text{constant}, \quad (5)$$

where P is the hydrostatic pressure, $0.5\rho v^2$ is the hydrodynamic pressure (i.e. the potential pressure invested in the movement of the water) and $\rho g z$ is the manometric height (ρ is the water density, g is gravitational acceleration and z is the distance between the surface and flow) (Vogel, 1994). For examination of flow in the horizontal plane, manometric height can be ignored, and the sum of hydrostatic and hydrodynamic pressure is referred to as the 'total head' (H_{tot}):

$$H_{tot} = P + 0.5\rho v^2 = \text{constant}. \quad (6)$$

Prior to water entering the mouth, the total head is in the form of dynamic pressure ($=0.5\rho v^2$) and is thus dependent on swimming speed. However, as water enters the mouth, its velocity slows and dynamic pressure decreases while the static pressure rises proportionally. Engineering experience and analysis of tuna ram ventilation suggest that pressure drop in the buccal cavity (ΔP_{bc}) is approximately 15% of the dynamic pressure (Brown and Muir, 1970). This drop is associated with the friction of water flow contacting the walls of the mouth and the gill arches. As water passes into the interlamellar spaces, a further drop in pressure occurs and is estimated by Poiseuille's equation for laminar channel flow:

$$\Delta P_{lc} = (12\mu v_{lc} l) / d^2, \quad (7)$$

where μ is the dynamic viscosity of seawater, v_{lc} is the velocity of water through the lamellar channels, l is lamellar channel length and d is lamellar channel width (Brown and Muir, 1970). In the elasmobranch gill, water exits the interlamellar spaces into a septal channel, and because of its complex morphology (i.e. septal channel diameter increases as it extends towards the gill slits and post-lamellar water is entrained along its entire length, Fig. 1A,B), the pressure differential associated with this flow cannot easily be assessed using the velocity–pressure relationships of hydrodynamics. However, knowing the total pressure differential (ΔP_{tot}) and that of the buccal cavity and lamellar channels, pressure drop associated with septal channel flow (ΔP_{sc}) is estimated by:

$$\Delta P_{sc} = \Delta P_{tot} - (\Delta P_{bc} + \Delta P_{lc}). \quad (8)$$

Estimated in this way, septal channel pressure drop accounts for approximately 80% of the total pressure differential.

Table 1 shows that the total pressure drop across the branchial apparatus is greater than H_{tot} estimated using Eqn 6. This indicates a negative pressure at the gill slits (P_{gs}) that helps to pull water through the branchial apparatus and works in conjunction with the dynamic pressure entering the mouth to induce ventilatory water flow. The magnitude of this negative pressure, which results from the acceleration of water around the body of the swimming shark, is estimated by subtracting the total measured pressure differential from H_{tot}; the mean for the six mako individuals is –18.1±2.5 Pa (Table 1). The ratio of P_{gs} to H_{tot} (i.e. the dimensionless pressure coefficient, C_p) is –0.24±0.04, which is similar to the pressure coefficient measured near the opercula of swimming bluefish, *Pomatomus saltarix* (Dubois et al., 1974), and has been replicated using streamlined objects mounted in a water tunnel (Vogel, 1994).

Comparison of ventilatory flow and branchial resistance in lamnids and tunas

Because the volume of the ventilatory stream can be adjusted through changes in swimming speed, mouth gape and, presumably, the size of the gill slits or opercular openings, it is not surprising that water flow parameters within the interlamellar channels of the mako are similar to those reported for skipjack tuna, despite differences in the body size of the specimens studied and distinctions in gill morphology. Estimates of the interlamellar water velocity (0.22±0.03 cm s^{-1}), residence time (0.79±0.14 s) and Re (0.06±0.01) for makos in this study (4.62–7.34 kg) swimming at 38.8±5.8 cm s^{-1} are similar to estimates for a 1.67 kg skipjack tuna swimming at its preferred (basal) speed of 66 cm s^{-1} (v_{lc}=0.29 cm s^{-1}, residence time=0.41 s, Re=0.03) (Brown and Muir, 1970; Stevens and Lightfoot, 1986). The slightly longer contact time of the mako ventilatory stream with the respiratory exchange surfaces likely reflects the increased width (=longer diffusion distance) of mako interlamellar channels. Thus, despite longer diffusion distances, the slightly increased residence time of mako interlamellar flow results in a relatively high oxygen utilization (53.4±4.2%) that is strikingly similar to that of tunas (range 44.3–56.0%) (Stevens, 1972; Bushnell and Brill, 1991; Bushnell and Brill, 1992).

The total pressure differentials driving branchial flow in makos and skipjack tuna are also fairly similar when swimming at their basal speeds. For a 1.67 kg skipjack tuna swimming at 66 cm s^{-1}, Brown and Muir (Brown and Muir, 1970) estimated a total branchial pressure drop of approximately 110 Pa. *In vivo* measurements made by Stevens (Stevens, 1972) and further analyzed by Stevens and Lightfoot (Stevens and Lightfoot, 1986) suggest that this is a reasonable estimate. For makos, a mean pressure gradient of 96.8±26.1 Pa was observed at a preferred swimming speed of 38.8 cm s^{-1} (Table 1). Although ΔP_{tot} is thus comparable for tunas and the mako at basal swimming speeds, the distribution of pressure drop within the branchial chamber varies greatly. In skipjack, 80 Pa (73% of the total resistance) is incurred as water passes through the interlamellar channels (Brown and Muir, 1970), as opposed to 14.4 Pa (15% of total resistance) in the mako (Table 1). Given that interlamellar water-flow velocities are similar, Eqn 7 suggests that the lower mako pressure drop at this location is primarily attributed to its wider interlamellar spaces [55.82±3.64 μm for makos in this study (Table 1), 20 μm for skipjack tuna (Brown and Muir, 1970)]. This increased spacing appears to be a needed compensatory mechanism for the high resistance incurred at the septal channels (77.0±23.6 Pa, 80% of mako total branchial resistance), a feature not present in the gills of tunas (Table 1).

This study thus provides evidence that the septal channel of the elasmobranch gill significantly contributes to gill resistance and is compensated by an increased lamellar spacing to reduce resistance through the interlamellar channels. This, in turn, limits lamellar frequency and, ultimately, the gill surface area of the mako and other lamnids in comparison to tunas. Specifically, the interlamellar channel width in the mako is approximately twice that of tunas,

resulting in one-half the lamellar frequency and one-half the gill surface area (Wegner et al., 2010b). This smaller respiratory area results in a lower volume of water that can be processed by the gills per unit time and this likely contributes to a reduced aerobic capacity in lamnids when compared with tunas, as manifested by lower aerobic enzyme activities, smaller amounts of red muscle and reduced sustainable swimming speeds (Bernal et al., 2003a; Bernal et al., 2003b; Sepulveda et al., 2007).

ACKNOWLEDGEMENTS

We thank D. Cartamil, D. Head, C. Jew, D. Kacev, E. Kisfaludy, A. Nosal, C. Peters, C. Sepulveda, J. Strother and K. Uyeji for help with various aspects of this project. We also thank E. Don Stevens and one anonymous reviewer for their comments.

FUNDING

This research was supported by National Science Foundation [grant no. IOS-0817774 to. J.B.G. and N.C.W.], the Tuna Industry Endowment Fund at Scripps Institution of Oceanography [to N.C.W.], and the Moore Family Foundation [to J.B.G.]. N.C.W. was supported by the Nadine A. and Edward M. Carson Scholarship awarded by the Achievement Rewards for College Scientists (ARCS), Los Angeles Chapter, and the National Science Foundation.

REFERENCES

Altringham, J. D. and Block, B. A. (1997). Why do tuna maintain elevated slow muscle temperatures? Power output of muscle isolated from endothermic and ectothermic fish. *J. Exp. Biol.* **200**, 2617-2627.

Bernal, D., Dickson, K. A., Shadwick, R. E. and Graham, J. B. (2001a). Review: analysis of the evolutionary convergence for high performance swimming in lamnid sharks and tunas. *Comp. Biochem. Physiol.* **129A**, 695-726.

Bernal, D., Sepulveda, C. A. and Graham, J. B. (2001b). Water-tunnel studies of heat balance in swimming mako sharks. *J. Exp. Biol.* **204**, 4043-4054.

Bernal, D., Sepulveda, C., Mathieu-Costello, O. and Graham, J. B. (2003a). Comparative studies of high performance swimming in sharks. I. Red muscle morphometrics, vascularization and ultrastructure. *J. Exp. Biol.* **206**, 2831-2843.

Bernal, D., Smith, D., Lopez, G., Weitz, D., Grimminger, T., Dickson, K. and Graham, J. B. (2003b). Comparative studies of high performance swimming in sharks II. Metabolic biochemistry of locomotor and myocardial muscle in endothermic and ectothermic sharks. *J. Exp. Biol.* **206**, 2845-2857.

Blank, J. M., Farwell, C. J., Morrissette, J. M., Schallert, R. J. and Block, B. A. (2007). Influence of swimming speed on metabolic rates of juvenile Pacific bluefin tuna and yellowfin tuna. *Physiol. Biochem. Zool.* **80**, 167-177.

Brill, R. W. (1979). Effect of body size on the standard metabolic rate of skipjack tuna, *Katsuwonus pelamis*. *Fish. Bull.* **77**, 494-498.

Brill, R. W. (1987). On the standard metabolic rates of tropical tunas, including the effect of body size and acute temperature change. *Fish. Bull.* **85**, 25-36.

Brill, R. W. and Bushnell, P. G. (1991). Metabolic and cardiac scope of high-energy demand teleosts, the tunas. *Can. J. Zool.* **69**, 2002-2009.

Brown, C. E. and Muir, B. S. (1970). Analysis of ram ventilation of fish gills with application to skipjack tuna (*Katsuwonus pelamis*). *J. Fish. Res. Board Can.* **27**, 1637-1652.

Bushnell, P. G. and Brill, R. W. (1991). Responses of swimming skipjack (*Katsuwonus pelamis*) and yellowfin (*Thunnus albacares*) tunas to acute hypoxia, and a model of their cardiorespiratory function. *Physiol. Zool.* **64**, 887-911.

Bushnell, P. G. and Brill, R. W. (1992). Oxygen-transport and cardiovascular-responses in skipjack tuna (*Katsuwonus pelamis*) and yellowfin tuna (*Thunnus albacares*) exposed to acute-hypoxia. *J. Comp. Physiol. B.* **162**, 131-143.

Carey, F. G., Teal, J. M., Kanwisher, J. W., Lawson, K. D. and Beckett, J. S. (1971). Warm-bodied fish. *Amer. Zool.* **11**, 137-145.

Dewar, H. and Graham, J. B. (1994). Studies of tropical tuna swimming performance in a large water tunnel. I. Energetics. *J. Exp. Biol.* **192**, 13-31.

Donley, J. M., Sepulveda, C. A., Konstantinidis, P., Gemballa, S. and Shadwick, R. E. (2005). Patterns of red muscle strain activation and body kinematics during steady swimming in a lamnid shark, the shortfin mako *Isurus oxyrinchus*. *J. Exp. Biol.* **208**, 2377-2387.

Dowis, H. J., Sepulveda, C. A., Graham, J. B. and Dickson, K. A. (2003). Swimming performance studies on the eastern Pacific bonito *Sarda chiliensis*, a close relative of the tunas (family Scombridae). II. Kinematics. *J. Exp. Biol.* **206**, 2749-2758.

Dubois, A. B., Cavagna, G. A. and Fox, R. S. (1974). Pressure distribution on the body surface of swimming fish. *J. Exp. Biol.* **60**, 581-591.

Emery, S. H. and Szczepanski, A. (1986). Gill dimensions in pelagic elasmobranch fishes. *Biol. Bull.* **171**, 441-449.

Graham, J. B. and Dickson, K. A. (2001). Anatomical and physiological specializations for endothermy. In *Fish Physiology*, Vol. 19 (ed. B. A. Block and E. D. Stevens), pp. 121-165. San Diego, CA: Academic Press.

Graham, J. B., Koehrn, F. J. and Dickson, K. A. (1983). Distribution and relative proportions of red muscle in scombrid fishes: consequences of body size and relationships to locomotion and endothermy. *Can. J. Zool.* **61**, 2087-2096.

Graham, J. B., Dewar, H., Lai, N. C., Lowell, W. R. and Arce, S. M. (1990). Aspects of shark swimming performance determined using a large water tunnel. *J. Exp. Biol.* **151**, 175-192.

Korsmeyer, K. E. and Dewar, H. (2001). Tuna metabolism and energetics. In *Fish Physiology*, Vol. 19 (ed. B. A. Block and E. D. Stevens), pp. 35-78. San Diego, CA: Academic Press.

Muir, B. S. and Hughes, G. M. (1969). Gill dimensions for three species of tunny. *J. Exp. Biol.* **51**, 271-285.

Sepulveda, C. A., Dickson, K. A. and Graham, J. B. (2003). Swimming performance studies on the eastern Pacific bonito *Sarda chiliensis*, a close relative of the tunas (family Scombridae). I. Energetics. *J. Exp. Biol.* **206**, 2739-2748.

Sepulveda, C. A., Graham, J. B. and Bernal, D. (2007). Aerobic metabolic rates of swimming juvenile mako sharks, *Isurus oxyrinchus*. *Mar. Biol.* **152**, 1087-1094.

Stevens, E. D. (1972). Some aspects of gas exchange in tuna. *J. Exp. Biol.* **56**, 809-823.

Stevens, E. D. and Lightfoot, E. N. (1986). Hydrodynamics of water flow in front of and through the gills of skipjack tuna. *Comp. Biochem. Physiol.* **83**, 255-259.

Vogel, S. (1994). *Life in Moving Fluids: the Physical Biology of Flow*. Princeton, NJ: Princeton University Press.

Wegner, N. C., Sepulveda, C. A., Bull, K. B. and Graham, J. B. (2010a). Gill morphometrics in relation to gas transfer and ram ventilation in high-energy demand teleosts: Scombrids and billfishes. *J. Morphol.* **271**, 36-49.

Wegner, N. C., Sepulveda, C. A., Olson, K. R., Hyndman, K. A. and Graham, J. B. (2010b). Functional morphology of the gills of the shortfin mako, *Isurus oxyrinchus*, a lamnid shark. *J. Morphol.* **271**, 937-948.